BIOCHEMISTRY
including biophysical chemistry & molecular biology

ARTICLE

pubs.acs.org/biochemistry

[NiFe] and [FeS] Cofactors in the Membrane-Bound Hydrogenase of *Ralstonia eutropha* Investigated by X-ray Absorption Spectroscopy: Insights into O_2-Tolerant H_2 Cleavage

Johannes Fritsch,[†] Simone Löscher,[‡] Oliver Sanganas,[‡] Elisabeth Siebert,[§] Ingo Zebger,[§] Matthias Stein,[∥] Marcus Ludwig,[†] Antonio L. De Lacey,[⊥] Holger Dau,[‡] Bärbel Friedrich,[†] Oliver Lenz,[†] and Michael Haumann*[,‡]

[†]Humboldt-Universität zu Berlin, Institut für Biologie/Mikrobiologie, 10115 Berlin, Germany

[‡]Freie Universität Berlin, Institut für Experimentalphysik, 14195 Berlin, Germany

[§]Technische Universität Berlin, Max-Volmer Institut, 10623 Berlin, Germany

[∥]Max-Planck-Institut für Dynamik komplexer technischer Systeme, 39106 Magdeburg, Germany

[⊥]Instituto de Catálisis y Petroleoquímica (CSIC), 28049 Madrid, Spain

Supporting Information

ABSTRACT: Molecular features that allow certain [NiFe] hydrogenases to catalyze the conversion of molecular hydrogen (H_2) in the presence of dioxygen (O_2) were investigated. Using X-ray absorption spectroscopy (XAS), we compared the [NiFe] active site and FeS clusters in the O_2-tolerant membrane-bound hydrogenase (MBH) of *Ralstonia eutropha* and the O_2-sensitive periplasmic hydrogenase (PH) of *Desulfovibrio gigas*. Fe-XAS indicated an unusual complement of iron−sulfur centers in the MBH, likely based on a specific structure of the FeS cluster proximal to the active site. This cluster is a [4Fe4S] cubane in PH. For MBH, it comprises less than ∼2.7 Å Fe−Fe distances and additional longer vectors of ≥3.4 Å, consistent with an Fe trimer with a more isolated Fe ion. Ni-XAS indicated a similar architecture of the [NiFe] site in MBH and PH, featuring Ni coordination by four thiolates of conserved cysteines, i.e., in the fully reduced state (Ni-SR). For oxidized states, short Ni−μO bonds due to Ni−Fe bridging oxygen species were detected in the Ni-B state of the MBH and in the Ni-A state of the PH. Furthermore, a bridging sulfenate (CysSO) is suggested for an inactive state (Ni_{ia}-S) of the MBH. We propose that the O_2 tolerance of the MBH is mainly based on a dedicated electron donation from a modified proximal FeS cluster to the active site, which may favor formation of the rapidly reactivated Ni-B state instead of the slowly reactivated Ni-A state. Thereby, the catalytic activity of the MBH is facilitated in the presence of both H_2 and O_2.

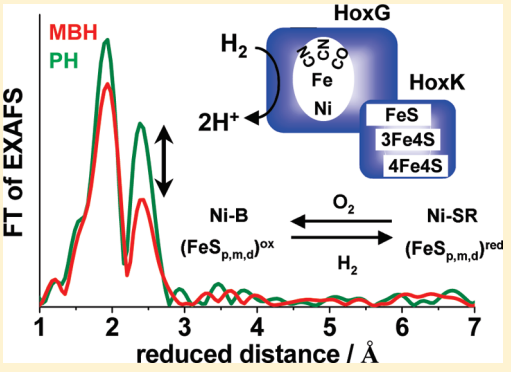

Hydrogenases (H_2ases) are enzymes that catalyze the cleavage and production of molecular hydrogen (H_2) at high turnover rates.[1,2] They are of interest in the worldwide effort to substitute fossil fuels by renewable energy sources, such as H_2.[3−5] A limitation for biotechnological application of most H_2ases is their sensitivity to dioxygen (O_2).[6] However, a few H_2ases are catalytically active in the presence of O_2.[7−11] The elucidation of the molecular basis of their O_2 tolerance may open new strategies to improve the catalytic features of O_2-sensitive H_2ases by genetic engineering[12−15] and could be useful for the design of novel biomimetic synthetic catalysts.[16−18]

The facultative chemolithoautotrophic bacterium *Ralstonia eutropha* H16 (*Re*) has the ability to grow on H_2, CO_2, and O_2 and harbors three H_2ases, all of which are active in the presence of O_2. These are the regulatory H_2ase (RH), which acts as a H_2 sensor,[19−21] the soluble NAD^+-reducing H_2ase (SH),[22−24] and the membrane-bound H_2ase (MBH).[25,26] All enzymes belong to the [NiFe] class, and their active sites contain one Ni atom and one Fe atom[1,27−29] as opposed to the [FeFe] H_2ases possessing a homometallic center.[1,27,30] The MBH, which is in the focus of this study, is bound to the periplasmic side of the cytoplasmic membrane via a membrane-integral *b*-type cytochrome.[31] The enzyme shows high H_2 oxidation activity[26] and feeds the derived electrons into the respiratory chain.[32]

The MBH sustains the growth of *R. eutropha* with H_2 even at atmospheric levels of O_2.[26,33−35] Electrochemical experiments have shown that H_2 oxidizing activity at ambient O_2 pressure (∼230 mbar) can be up to 60% of the activity determined in the

Received: March 11, 2011
Revised: May 27, 2011
Published: May 27, 2011

absence of O_2; nearly full activity is recovered at high redox potentials when O_2 is replaced with H_2.[33−36] Furthermore, the MBH is insensitive to inhibition by CO.[36] These features are unique and not found for the standard type of [NiFe] H_2ases, e.g., from *Desulfovibrio* and *Allochromatium* species, in which H_2 oxidizing activity is completely inhibited by traces of O_2 and low CO levels. Reactivation of O_2-inhibited standard H_2ases occurs extremely slowly and only at low potentials.[6,37,38]

The high O_2 tolerance of the MBH is surprising because its amino acid sequence[26,29] suggests a high degree of structural similarity with standard [NiFe] H_2ases, e.g., the periplasmic H_2ase (PH) of *Desulfovibrio gigas* (Figure 1). The MBH consists of a large subunit (HoxG) comprising the [NiFe] site and a small subunit (HoxK), which harbors binding sites for three FeS clusters (Figure 1).[39,40] According to the crystal structures of several [NiFe] hydrogenases, generally four conserved cysteines in the large subunit are involved in coordinating the active site Ni and Fe atoms.[27,41] A further common feature of [NiFe] H_2ases is the ligation of the Fe by two cyanides (CN^-) and one CO as observed by FTIR spectroscopy.[36,42,43] Apart from these similarities, biochemical, electrochemical, and spectroscopic results[26,33,36,43−45] suggest that O_2 tolerance of the MBH is related to the structural arrangement of its metal cofactors, rather than to the restricted access of O_2 and CO to the [NiFe] site because of a narrow gas channel as proposed for H_2-sensing H_2ases.[12,26,46] Notably, compared to standard H_2ases, biosynthesis of active MBH requires a significantly larger set of maturation proteins.[47−49]

Spectroscopic studies of the MBH using EPR and FTIR techniques uncovered several features differing from those of standard enzymes.[43−46] The so-called Ni-A state, corresponding to the oxidized, inactive unready enzyme, could not be detected in wild-type MBH. For standard H_2ases residing in the Ni-A state, a (hydro)peroxo species was suggested to occupy the bridging position between Ni and Fe, whereas in the Ni-B state, a hydroxide is assigned as a bridging ligand.[50] Remarkably, in addition to the absence of Ni-A, a complex EPR spectrum indicates modification of the FeS cluster in the position proximal to the [NiFe] site in the MBH.[43−46] The structural basis of these modifications needs to be elucidated.

In this study, the metal centers of the MBH were characterized by an element-specific technique, namely X-ray absorption spectroscopy (XAS),[51,52] by which the coordination environment and redox changes of the protein-bound metal atoms were determined. The spectroscopic features of the MBH are compared to those of the PH standard H_2ase, for which crystal structures are available.[27,53] Our results suggest a different structure of the proximal FeS cluster, but a rather similar although more disordered [NiFe] active site in MBH compared to that in PH.

MATERIALS AND METHODS

Enzyme Purification and Sample Preparation. Three different MBH protein preparations were used for this study. The most active MBH (mean activity of 140 ± 13 units/mg) was isolated from *R. eutropha* strain HF649, which was grown on fructose-glycerol mineral medium under oxygen-limited conditions.[43,44,54] The membrane fraction was prepared under an argon atmosphere and oxidized by the addition of 50 mM $K_3[Fe(CN)_6]$ prior to aerobic solubilization with Triton X-114. Purification via *Strep*-Tactin affinity chromatography was conducted in K-PO_4 buffer (pH 7.0). The protein samples were

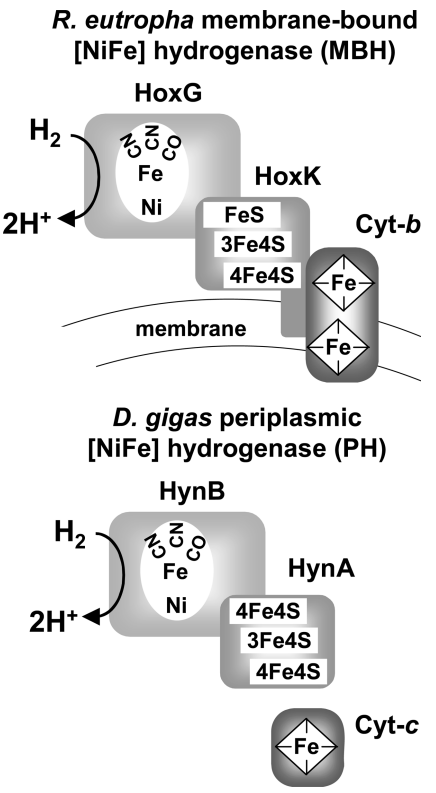

Figure 1. Composition of [NiFe] hydrogenases of the standard type (PH) from *D. gigas*[53] and of the membrane-bound type (MBH) from *R. eutropha*.[25,31] Two CN^- groups and one CO group at the active site iron were inferred by FTIR.[43] The enzyme preparations lacked the membrane and the cytochrome *b* subunit with its two heme groups in the case of MBH and cytochrome *c* in the case of PH. FeS denotes a modified proximal cluster in the MBH.

concentrated using Amicon Ultra-15 (PL-30) and Amicon Microcon (YM-30) filtration devices (Millipore) in buffer containing 40 mM K-PO_4 (pH 5.5), 150 mM NaCl, and 20% glycerol. MBH mutant protein (HoxK Cys19/120Gly) was prepared as previously described[54] and concentrated as shown above (pH 5.5, ~86 units/mg). Less active MBH protein (mean activity of 60 ± 4 units/mg) was purified as described previously[26,43] and concentrated under aerobic conditions, and the purified protein was finally stored in 50 mM K-PO_4 buffer (pH 8.0). All preparations lacked the membrane-integral cytochrome *b* that serves as the primary electron acceptor. Protein concentrations were determined by the Bradford method[55] with bovine serum albumin as a standard. The purity of samples was examined by sodium dodecyl sulfate−polyacrylamide gel electrophoresis. The H_2ase activity was determined photometrically[26,40] in 50 mM K-PO_4 buffer (pH 5.5) using the artificial electron acceptor methylene blue. For treatments in the presence of H_2, concentrated protein solutions (~30 μL) were enclosed in gastight reaction vessels, the atmosphere was exchanged by repeated degassing,[23] and solutions were incubated under a gentle stream of moist gas for 10−45 min at ~20 °C. The final MBH protein concentrations in the samples were 0.5−0.8 mM. PH protein from *D. gigas* was prepared and concentrated under aerobic conditions, and protein concentrations were determined as described previously.[56] Activation of PH was performed upon incubation of Eppendorf reaction vessels containing concentrated protein (~30 μL) in repeatedly degassed

dx.doi.org/10.1021/bi200367u |*Biochemistry* 2011, 50, 5858–5869

buffer at 35 °C under pure H_2 for 90−180 min. Reduction of PH was achieved by incubation with sodium dithionite (10 mM) for 20 min. Final PH concentrations were 0.7−1.0 mM. Immediately after the treatments, ∼20 μL of protein samples was transferred under an argon atmosphere to Kapton-covered sample holders for XAS and EPR measurements, rapidly frozen, and stored in liquid nitrogen until use.

Metal Content Quantification. The metal content of H_2ase proteins was determined by total-reflection X-ray fluorescence detection (TXRF)[57] on a PicoFox instrument (Bruker). Ni and Fe concentrations were determined using the built-in spectrometer functions relative to a gallium standard (Sigma), which had been added to the protein solutions prior to the measurements.

FTIR Spectroscopy. Infrared spectroscopy was conducted on a Bruker TENSOR 27 spectrometer as described previously[43,44] with aliquots of the protein samples used for XAS.

X-ray Absorption Spectroscopy (XAS). XAS measurements were performed on beamline D2 of the EMBL outstation (at HASYLAB, DESY, Hamburg, Germany) and beamline KMC-1 of BESSY (Helmholtz-Zentrum, Berlin, Germany). K_α fluorescence-detected XAS spectra at the Ni and Fe K-edges were collected for samples held in liquid helium cryostats at 20 K with energy-resolving 13-element Ge detectors (Canberra).[58,59] Fe spectra were recorded for a monochromator scan range of 7000−8200 eV. For Ni, in an extended-range approach,[60] the scan range was 8200−9200 eV. XAS spectra were averaged (5−12 scans) after energy calibration of each scan by the Bragg reflection method[61] or using the spectra of Ni or Fe metal foils as energy standards, normalized, and EXAFS oscillations were extracted.[52] The energy scale of EXAFS spectra was converted to a wavevector (k) scale using E_0 values of 8333 eV (Ni) and 7112 eV (Fe). E_0 refined to ∼7120 eV (Fe) and ∼8336 eV (Ni), respectively, in the simulations. Unfiltered k^3-weighted spectra were used for least-squares curve fitting and Fourier transform (FT) calculation with the in-house program SimX.[52] In EXAFS simulations, phase functions from FEFF7[62] and amplitude reduction factors (S_0^2) of 0.9 (Ni) and 0.85 (Fe) were used, which were chosen because they reproduced the known coordination numbers in simulations of EXAFS data of model Ni and Fe complexes (not shown). The fit ranges for k^3-weighted EXAFS data were 1.6−16.1 Å^{-1} for Fe and 2−15 Å^{-1} for Ni. The distance resolution of EXAFS data may be calculated according to the relationship $\Delta R = \pi/2\Delta k$, with Δk being the k range of data in the simulation. For the ranges mentioned above, the resolution was estimated to be ∼0.1 Å for Fe and ∼0.12 Å for Ni data, which is less than the distance spread found in the fits of the EXAFS data of the hydrogenases. The development of satisfactory simulation models for the EXAFS data involved gradual refinement of the fit approach by the inclusion of additional metal−backscatterer shells. The results of a simple fit and a more complex fit, revealing additional structural details, are shown for Fe, and one fit for Ni data is shown in Results, which provided the lowest fit errors (for the more complex fit for Fe) for a reasonably low number of unrestricted fit parameters. The given error sum (R_F) is defined as the deviation in percent between the Fourier-filtered k space EXAFS data in the fit range and the fit curve;[52] values around 10% reveal a very high fit quality.

XANES Simulations. XANES calculations were conducted as described in refs 23 and 63 using the code FEFF8.2[62] with the full-multiple-scattering (FMS) and the self-consistent-field (SCF) options activated. Atomic coordinates of FEFF input files were generated using the crystal structure of the [NiFe] site of *D. gigas* H_2ase[41] as a template and Ni−ligand distances from the EXAFS analysis. Calculated spectra were shifted by 1 eV to lower energies and smoothed over data points within 3 eV for better comparison with the experimental data.

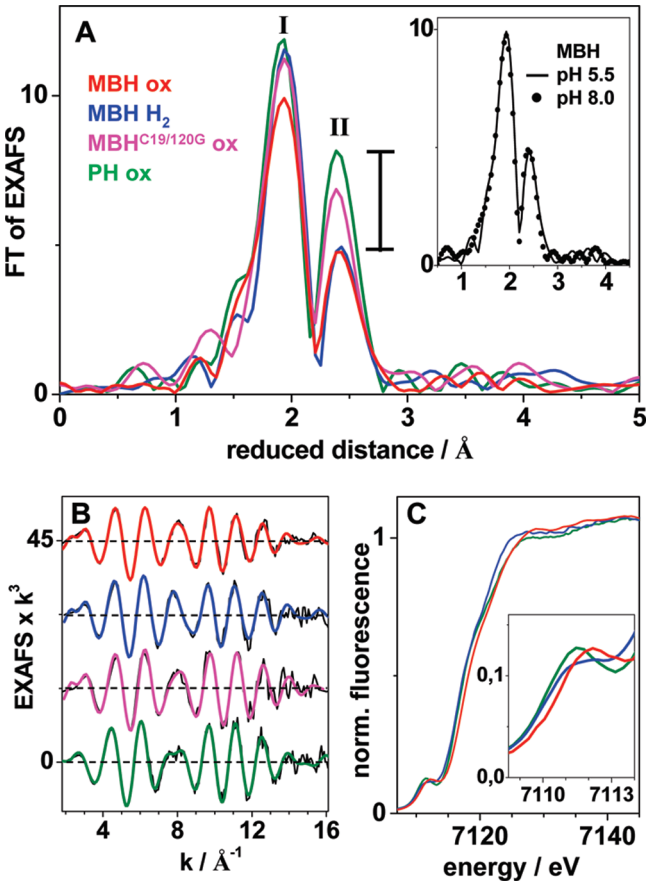

Figure 2. Fe-XAS spectra. (A) Fourier transforms (FTs) of EXAFS spectra (in panel B) of oxidized (red) and H_2-reduced (blue) MBH, of the HoxK C19G/C120G mutant of MBH (magenta), and of oxidized PH (green). The bar marks the difference between FT peak amplitudes due to Fe−Fe vectors in wild-type MBH and PH. The inset shows the FTs of MBH at pH 5.5 (line) and of the less active MBH preparation at pH 8 (dots). FTs were calculated for a k range of 2−16 Å^{-1} and using cos^2 windows over 10% at both k range ends. (B) Experimental EXAFS spectra (black) and simulations (colored lines) with parameters listed in Table 1 (fits I, VI, VIII, and IX). (C) Respective Fe K-edge spectra and their pre-edge features on an expanded energy scale in the inset.

Density Functional Theory (DFT) Calculations. DFT calculations have successfully been applied to [NiFe] hydrogenase active site models (for reviews see refs 64, 65). Here, calculations were performed using ORCA3.[66] Geometry optimizations of [NiFe] site models involved the BP86 exchange correlation functional[67,68] and a double-ζ basis set[69] with polarization functions from the TURBOMOLE library (ftp://ftp.chemie.uni-karlsruhe.de/pub/basen) and a dielectric constant ε of 4 in a COSMO solvation model.[70,71]

RESULTS

The FeS Clusters Studied by XAS at the Iron K-Edge. By Fe-XAS, we compared the properties of FeS clusters in the *R. eutropha* MBH with those of the *D. gigas* PH (Figure 2). In the XANES

spectrum of oxidized MBH, the primary maximum at ~7129 eV was larger, the edge energy at the 50% level was ~0.6 eV higher (7118.2 eV), and the energy of the pre-edge feature due to 1s → 3d electronic transitions was ~0.4 eV higher (7112.1 eV), compared to the respective parameters of the PH spectrum (Figure 2C). These differences suggest alterations in the average iron coordination and an overall higher content of oxidized Fe ions in the MBH. In H_2-reduced MBH, the edge and pre-edge features were shifted by ~0.9 and ~0.6 eV, respectively, to lower energies (7117.3 and 7111.5 eV, respectively), indicating significant Fe reduction in this sample (Figure 2C).

By TXRF, an Fe:Ni ratio of 12.1 ± 0.3 was determined for the PH, which is in agreement with the expected value of 12 Fe ions per Ni (deduced from two [4Fe4S] clusters, one [3Fe4S] cluster, and the active site). For the MBH, a slightly lower ratio of 11.1 ± 0.8 was determined. However, even a small Ni contamination of 5% of the protein-bound metal would diminish the ratio by ~0.5 units and result in an underestimation of the metal ratio. Thus, a conservative estimate is a content of 12 Fe ions for the MBH, similar to that of the PH. Taking into account this value and an expected edge shift of ~3 eV for a single-electron redox change of a monoiron compound,[72] we find the data are compatible with the presence of one to two more oxidized ions, i.e., Fe(III), in the oxidized MBH compared to the PH and with the reduction of approximately three iron ions from Fe(III) to Fe(II) in the case of the MBH upon H_2 incubation.

EXAFS analysis was employed to study the structure of the Fe sites (Figure 2). The Fourier transforms (FTs) of the respective EXAFS spectra of oxidized MBH and PH were dominated by FeS cluster contributions, exhibiting two distinct FT peaks related to Fe−S (I) and Fe−Fe (II) distances.[21,58] For the oxidized MBH, both FT peak amplitudes were largely diminished, suggesting an overall structure of the FeS clusters different from that in the PH. For H_2-reduced MBH, an increase in the magnitude of FT peak I was observed. However, peak II again was much smaller in magnitude than that for the PH (Figure 2A). Fe−Fe and Fe−ligand distances (R_i) and their numbers per Fe atom (coordination number N_i) were determined by curve fitting of the EXAFS oscillations.[48] The spectrum of the PH was in full agreement with the corresponding simulations (Table 1, I and II) predicting two [4Fe4S] clusters and one [3Fe4S] cluster in this enzyme. In particular, the coordination number (N_{Fe-Fe}) of Fe−Fe distances of ~2.7 Å, typical for the FeS clusters mentioned above, closely matched the value of ~2.6, which was calculated for the PH (see below). In addition, the interatomic distances were similar to those in crystal structures[53] and previous XAS data.[73]

Simulation of the EXAFS spectrum of oxidized MBH using the same FeS complement as for the PH was insufficient [2-fold increased error, R_F (Table 1, III)]. A better fit quality was obtained using the Debye−Waller parameters ($2\sigma^2$) of the PH as a reference but varying the individual N_i values (Table 1, IV). A coordination number N_{Fe-Fe} of ~1.6 was obtained for the MBH, which is approximately 1 unit lower than that in the PH. A similar fit (not shown) was obtained for the less active MBH preparation at pH 8.0 (Figure 2A). Accordingly, major differences in the average iron coordination spheres in the two MBH preparations were not observed by XAS. The N_{Fe-Fe} value of the MBH appeared to be too low to accommodate two [4Fe4S] clusters and one [3Fe4S] cluster, suggesting an apparent diminishing of the Fe−Fe contributions to the MBH EXAFS by interference effects, e.g., of Fe−S and Fe−Fe interactions.

For the first-sphere iron coordination in MBH, an apparent number of Fe−S bonds was obtained that was also too small to account for the four sulfurs ligating the Fe ions in conventional FeS clusters (Table 1, III and IV). However, the number of interactions of iron with light scatterers due to the Fe−C (=O/N)/O bonds at the active site iron was similar for MBH and PH, and thus, there was no evidence of oxidatively modified FeS clusters in the MBH. A more elaborate EXAFS simulation approach included two Fe−S and Fe−Fe shells. This approach revealed additional longer iron−sulfur bonds of ~2.6 Å and thus a total N_{Fe-S} closer to the expected value of ~4, and an improved fit quality. Furthermore, the N_{Fe-Fe} value was increased to close to 2 (Table 1, V), which, however, still was significantly lower than that for the PH. Two Fe−Fe distances of 2.68 and 2.78 Å (with coordination numbers close to unity) and a longer distance of ~3.4 Å with a smaller coordination number then became discernible (Table 1, V and VI). The Debye−Waller parameter (σ) (Table 1) suggested a distance distribution of ±0.06 Å for the Fe−Fe interactions. Thus, particularly short Fe−Fe distances of ~2.6 Å and longer distances of ~2.85 Å presumably are present in the MBH, both of which were not detectable in the PH. However, the conventional Fe−Fe distance of ~2.7 Å was observed in both enzymes.

Simulations of the EXAFS of H_2-reduced MBH using the same approach yielded a similar N_{Fe-Fe} close to 2 like that for the oxidized enzyme (Table 1, VII and VIII). The increase in the magnitude of FT peak I was explained by homogenization of the Fe−S bond lengths, in agreement with the presence of a larger Fe(II):Fe(III) ratio in the reduced enzyme, which was also observed in the XANES.

Figure 2 shows also the EXAFS spectrum of an MBH variant, in which two cysteines (Cys19 and Cys120) were replaced with glycines in the small subunit HoxK by genetic engineering.[54] These particular cysteines are absent in the PH and appear to be located close to the proximal FeS cluster in the MBH. For the respective mutant protein, $MBH^{C19G/C120G}$, a significantly increased oxygen sensitivity has been reported previously.[54] The Fe:Ni ratio of $MBH^{C19G/C120G}$ preparations was 11.6 ± 0.3, which is close to the value of 12 Fe ions expected according to the *D. gigas* structure. The FT spectrum of the mutant protein in particular revealed an increased magnitude of peak II, more similar to that of the PH. Accordingly, the EXAFS simulation yielded a larger N_{Fe-Fe} for the ~2.7 Å distances than in wild-type MBH. In the mutant protein, the Fe−Fe distances did not exceed ~3.0 Å (Table 1, IX). In summary, the overall structure of FeS clusters in this MBH variant was significantly different from that in wild-type MBH and more similar to that in the PH.

For the PH, a total of 31 Fe−Fe or −Ni distances with a length of ~2.7 Å was calculated (each Fe−Fe pair contributes two distances; 2 × 12 + 1 × 6 distances in the two [4Fe4S] clusters and one [3Fe4S] cluster and the Ni−Fe distance with a similar length and therefore indistinguishable from the Fe−Fe interactions; see the next section). For the MBH, a comparable calculation based on 12 Fe ions and on the data displayed in Table 1 yielded ~25 Fe−Fe or −Ni distances of ~2.7 Å and approximately four longer vectors of ~3.4 Å. According to EPR results, the MBH contains one [4Fe4S] cluster, one [3Fe4S] cluster, and an additional FeS cluster of unknown structure.[43,45,54] Subtraction of the 18 Fe−Fe vectors of the [4Fe4S] and [3Fe4S] clusters and the Ni−Fe distance resulted in six Fe−Fe vectors of ~2.7 Å in addition to the longer interactions, which are likely attributed to the third FeS cluster. These

Table 1. Simulation Parameters of Fe EXAFS Spectra of PH and MBH[a]

sample	fit	shell	N_i (per Fe)	R_i (Å)	$2\sigma_i^2$ ($\times 10^3$ Å^2)	R_F (%)
PH ox	I	Fe−C	0.33[b]	2.08	2	9.8
		Fe−S	3.83[b]	2.28	7	
		Fe−Fe	2.58[b]	2.72	7	
	II	Fe−C	0.44	2.07	2[b]	8.5
		Fe−S	3.63	2.28	6	
		Fe−Fe	2.49	2.72	8	
MBH ox	III	Fe−O	0.33[b]	2.05	2[b]	18.0
		Fe−S	3.83[b]	2.28	9	
		Fe−Fe	2.58[b]	2.72	14	
	IV	Fe−O	0.57	2.06	2[b]	11.8
		Fe−S	3.17	2.29	7[b]	
		Fe−Fe	1.50	2.74	7[b]	
	V	Fe−O	0.58	2.06	2[b]	8.2
		Fe−S	3.37	2.29	7[b]	
		Fe−S	0.82	2.60	7[b]	
		Fe−Fe	1.85	2.72	7[b]	
		Fe−Fe	0.35	3.34	7[b]	
	VI	Fe−O	0.57	2.06	2[b]	8.9
		Fe−S	3.37	2.29	7+	
		Fe−S	0.91	2.61	7[b]	
		Fe−Fe	1.24	2.66	7[b]	
		Fe−Fe	0.88	2.79	7[b]	
MBH H_2	VII	Fe−O	0.35	2.13	2[b]	11.1
		Fe−S	3.78	2.31	7[b]	
		Fe−S	0.78	2.73	7[b]	
		Fe−Fe	1.81	2.74	7[b]	
		Fe−Fe	0.55	3.42	7[b]	
	VIII	Fe−O	0.43	2.13	2[b]	12.3
		Fe−S	3.73	2.31	7[b]	
		Fe−S	0.26	2.60	7[b]	
		Fe−Fe	1.08	2.69	7[b]	
		Fe−Fe	0.93	2.80	7[b]	
MBH C19G/ C120G ox	IX	Fe−O	0.48	2.07	2[b]	12.5
		Fe−S	3.68	2.28	7[b]	
		Fe−S	0.83	2.59	7[b]	
		Fe−Fe	2.36	2.72	7[b]	
		Fe−Fe	0.25	3.02	7[b]	

[a] C19G/C120G denotes a HoxK variant of the MBH;[54] ox stands for oxidized and H_2 for hydrogen-reduced proteins. N_i is the coordination number, R_i the Fe−backscatterer distance, and $2\sigma_i^2$ the Debye−Waller factor. [b] Fixed parameters in the fit procedure. For fit I, the N_i values for the PH were calculated by including (i) a set of two [4Fe4S] clusters and one [3Fe4S] cluster (the distal [4Fe4S] cluster is ligated by one N atom from a histidine), (ii) one Fe−Ni vector that was indistinguishable from the Fe−Fe distances, and (iii) coordination of the active site Fe by two CysS and three carbons from the two CN^- ligands and the CO. The R_F value[52] was calculated for reduced distances of 1−3 Å. Increasing fit numbers for a specific sample denote, for example, increasingly complex simulation approaches. The approximate errors in R and N values may be given as ∼0.02 Å and ∼10−20%, respectively, for distances of <3 Å and slightly larger for minor EXAFS contributions.[52]

values are incompatible with an assignment of this cluster to a conventional [4Fe4S] cubane in the MBH and suggest a more unusual FeS species, most probably in the proximal position.[43,45,54]

Ni XAS on the Active Site Structure. Prior to XAS analysis, the population of the various redox states of the [NiFe] site in the samples was determined by EPR and FTIR spectroscopic techniques (data not shown; see refs 42, 43, 45, 54, 74, and 75). EPR revealed that the oxidized PH was more than 85% in the Ni^{III}-A state, previously interpreted as carrying a bridging peroxide species between the Ni and Fe ions.[50,76] After reductive incubation with H_2 at 35 °C for 90 min, the Ni^{III}-C state with a hydride, H^-, in the bridging position[77,78] was present in ∼65% of the protein; minor populations of other states summed up to ∼35%. In sodium dithionite-reduced PH, most of the [NiFe] site was fully reduced[75,79] and the respective Ni^{II}-SR states (see below) may harbor a metal-bound hydride, as well.[64,80]

For the MBH, various states of the [NiFe] site have been previously assigned by FTIR spectroscopy, according to the characteristic infrared stretching frequencies of the Ni-bound CO [ν(CO)].[43,44,54,81] Analysis of the ν(CO) values of the anaerobically oxidized MBH samples at pH 5.5 revealed that the majority of the [NiFe] sites (∼70%) resided in the Ni^{III}-B state, while the remaining fraction contained Ni(II) states (Table 2). The Ni-A state was not detected in any of the studied MBH samples, which is consistent with previous observations.[43−45,54] In H_2-reduced MBH, the Ni-SR states were dominant (∼80%). The Ni_{ia}-S inactive state with a Ni(II)[43,54] was the main species (∼70%) observed in aerobically purified MBH at pH 8.0. An increased Ni_{ia}-S population was also found in a sample of highly active, H_2-reduced MBH that was reoxidized by being exposed to air after XAS data collection and subsequent thawing (Table 2).

The coordination environment and oxidation state of the Ni atom as a crucial constituent of the active site were studied by XAS at the Ni K-edge. XANES spectra of the PH in the Ni-A state and the MBH in the Ni-B state revealed a similar edge energy, in agreement with the presence of Ni(III) in both species (Figure 3). The edge shapes were typical for a dominant sulfur coordination of the Ni,[82] i.e., by the thiolates of four cysteine residues. The two enzymes showed only minor differences, suggesting a quite similar first-sphere Ni coordination. A PH sample with a preferential Ni-C content exhibited a decreased secondary edge maximum at ∼8360 eV, likely due to the replacement of the Ni−Fe bridging oxygen species with a hydride.[82−84] Interestingly, the slightly higher edge energy implied an even more oxidized Ni ion in the Ni-C state compared to the Ni-A state. Decreased secondary edge maxima also were observed for MBH and PH in the Ni-SR state(s). Because of near-quantitative Ni(II) formation, the corresponding edge energies were around 0.5 eV lower than in the oxidized samples (Figure 3). In the oxidized MBH at pH 8.0, a pronounced increase in the primary edge maximum at ∼8350 eV suggested additional terminal oxygen ligands at the Ni(II)[23,58,82,85] in the Ni_{ia}-S state and therefore a substantially different site structure compared to that of the Ni-B state.

Via application of EXAFS analysis, the bond lengths and numbers of ligands at the Ni ion were determined (Figure 4). The Fourier transform (FT) of the EXAFS spectrum (Figure 4A) of the PH in the Ni-A state revealed two main peaks due to Ni−oxygen and Ni−sulfur bonds. Features at longer distances reflected contributions from the Ni−Fe vector.[23,60] The best-fit parameters (Table 3, I) showed that the Ni-A spectrum was completely described by close to one short Ni−oxygen distance,

Table 2. Redox-State Populations of the [NiFe] Site in Various MBH Preparations[a]

state of [NiFe] site	Ni_r-B	Ni_{ia}-S	Ni-S (Ni_r-S, $Ni_{r/u}$-S)	Ni_a-C	Ni_a-SR (Ni_a-SR, Ni_a-SR′, Ni_a-SR′)
Ni oxidation state	III	II	II	III	II
ν(CO) (cm^{-1})	1948.0	1929.6	1933.8, 1944.7	1957.0	1944.7, 1926.2, 1918.0
oxidized, pH 5.5	71	0	28 (13, 15)	1[f]	0
H_2-reduced, pH 5.5	0	0	11 (11, 0)	10	79 (18, 50, 11)
air-reoxidized, pH 5.5	36[b]	20	41 (13, 28)	3[f]	0
oxidized, pH 8.0[e]	2[c]	69	26 (13,[d] 13)	3[f]	0

[a] Populations (in percent, error of approximately ±5%) were derived from Gaussian fits of the CO stretching vibrations in the FTIR absorbance spectra [not shown (see refs 43 and 44)]. The respective state assignments follow previous attributions.[43] Indices denote active (a), inactive (ia), ready (r), and unready states (u). The assignment of the 1944.7 cm^{-1} band is ambiguous; however, it belongs presumably to an oxidized EPR-silent state. [b] Band at 1950.6 cm^{-1}. [c] Band at 1948.9 cm^{-1}. [d] Band at 1935.9 cm^{-1}. [e] Values for the less active MBH preparation. [f] These minor contributions are presumably due to a further inactive Ni-S state.

four Ni−sulfur bonds from the cysteines at the active site, and a Ni−Fe distance of 2.75 Å, all of which are similar to those found in crystal structures.[50,53] The short bond length of 1.85 Å suggested that the O atom was in a Ni−Fe bridging position.[83] Further O atoms in the first coordination sphere of Ni were not detected. This rather excludes the presence of sulfenates (oxidized cysteines, CysSO) bound via their O atom to Ni, which have been found in several crystal structures of oxidized *Desulfovibrio* H_2ases.[86−88] Also, the second O atom of a (hydro)peroxide ligand, i.e., ∼2.2 Å from Ni, could not be observed. In the Ni-C sample of the PH (Figure 4A and Table 3, II), the Ni−oxygen bond was completely lost (vanishing N_{Ni-O}). The expected Ni−hydride bond[77,78] in the Ni-C state cannot be detected by EXAFS because of the very small backscattering amplitude of hydrogen. A similar overall coordination of the Ni(II) was also determined for the Ni-SR states of the PH (Table 3, III). The shortening of the Ni−Fe distance by ∼0.2 Å in Ni-C and Ni-SR was in agreement with crystal structures of reduced *Desulfovibrio* H_2ases.[86,88] In the Ni-SR state, the longest Ni−sulfur distance, which likely belongs to the axial sulfur ligand at Ni,[41] was even longer than the Ni−Fe distance, as previously observed.[14]

The FT of the EXAFS spectrum of the MBH in the Ni-B state was different from that of the PH in the Ni-A conformation. The considerably smaller overall amplitudes (Figure 4B) suggested more variable Ni−sulfur bond lengths in the MBH. A corresponding simulation revealed a coordination number of the Ni−oxygen interactions of ∼0.7 (Table 3, IV), in agreement with a Ni-B content of ∼70% in the respective sample. The main differences between the Ni-B state of the MBH and the Ni-A state of the PH were (i) an ∼0.03 Å longer Ni−oxygen distance, (ii) an ∼0.04 Å longer mean Ni−sulfur distance, (iii) a doubled Debye−Waller parameter ($2\sigma^2$) of the shorter Ni−sulfur interactions, which implied a larger Ni−sulfur distance distribution between 2.12 and 2.28 Å, and (iv) an ∼0.1 Å shorter Ni−Fe distance in the MBH of ∼2.65 Å (Table 3, IV).

The EXAFS spectrum of H_2-reduced MBH was very similar to that of sodium dithionite-reduced PH (Figure 4). The respective simulations revealed a similar Ni coordination in both samples and, in particular, the apparent absence of Ni-bound oxygen. The Ni−Fe distance was shortened by ∼0.15 Å (Table 3, V) and thereby became more easily discerned in the FT spectra (Figure 4B). The largely decreased $2\sigma^2$ value of the Ni−sulfur interactions indicated a homogenization of the corresponding bond lengths in the MBH in the Ni-SR state. However, the overall Ni−sulfur and Ni−Fe distances remained slightly longer than in the PH.

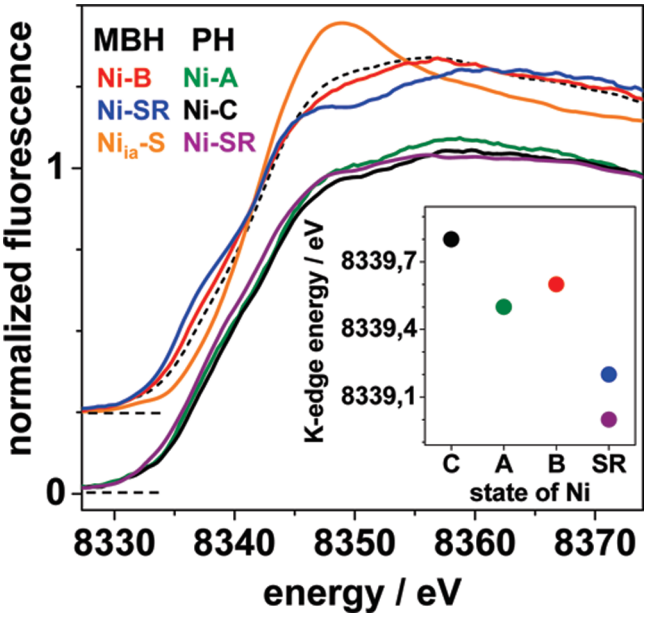

Figure 3. Ni K-edge spectra of MBH and PH samples containing mostly the indicated states of the [NiFe] site with formal Ni(III) (Ni-A, -B, and -C) or Ni(II) (Ni-SR and Ni_{ia}-S) oxidation states. The spectrum of an air-reoxidized MBH sample is shown as a dashed line. Spectra of MBH were vertically displaced. The inset shows K-edge energies at the 50% level of edge spectra.

The FT of the EXAFS spectrum of the MBH preparation preferentially in the Ni_{ia}-S state (pH 8.0) revealed largely diminished amplitudes, a shift of the main peak to larger distances, and a smaller peak feature due to short Ni−oxygen bonds compared to those in the Ni-B state (Figure 4B). The simulation yielded an increased number of Ni−oxygen bonds with a longer interatomic distance of ∼2 Å, an ∼0.1 Å longer mean Ni−sulfur bond length, an increase in the coordination number of long Ni−sulfur distances to approximately two, and an ∼0.3 Å longer Ni−Fe distance of ∼3.05 Å, compared to those of the Ni-B state of the MBH (Table 3, VI). The longer oxygen bonds most likely belong to terminal Ni ligands and not to metal-bridging μO species. Two long Ni−sulfur interactions may be attributable to the axial Ni−SCys bond and to a Ni−O(SCys) binding motif (see below).

The long Ni−Fe distance and additional long Ni−sulfur distances of the MBH in Ni_{ia}-S resembled the situation in crystal structures of standard [NiFe] H_2ases showing a Ni−Fe bridging

dx.doi.org/10.1021/bi200367u |*Biochemistry* 2011, 50, 5858–5869

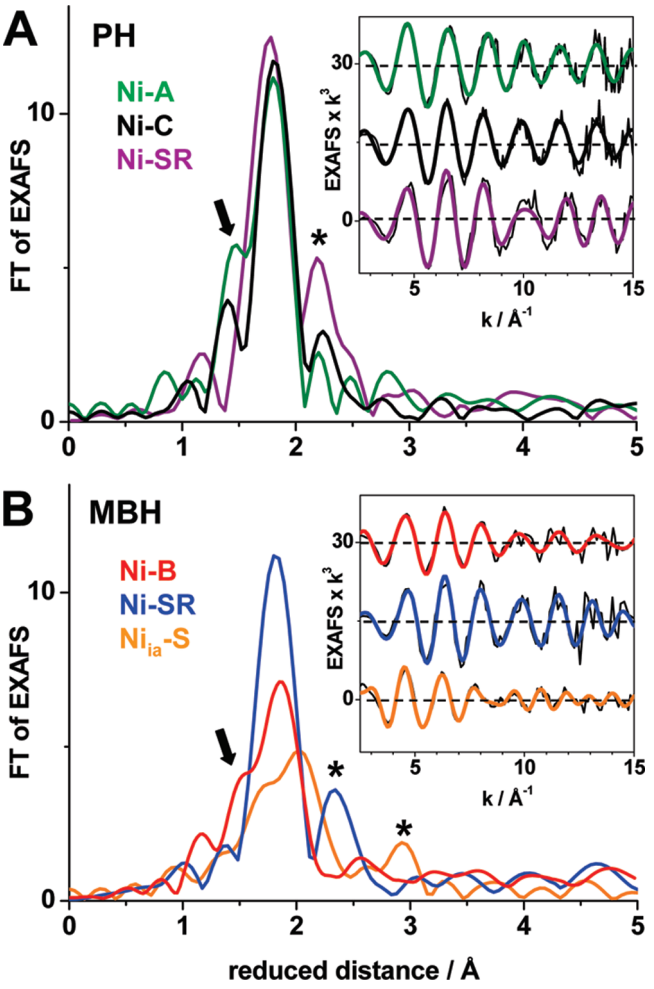

Figure 4. Ni EXAFS spectra. (A) FTs of spectra of PH in the oxidized (Ni-A), H_2-reduced (Ni-C), and sodium dithionite-reduced (Ni-SR) states. (B) FTs of spectra of MBH in the oxidized (Ni-B), H_2-reduced (Ni-SR), and inactive (Ni_{ia}-S) states. The arrows mark FT peaks due to Ni−μO bonds. Asterisks denote contributions from Ni−Fe vectors. FTs were calculated for a k range of 2−15 $Å^{-1}$ and using $\cos^2$ windows over 10% at both k range ends. Insets in panels A and B show the respective experimental EXAFS spectra (thin black lines) and their simulations (thick lines) with parameters in Table 3. All spectra are displayed on the same scale.

sulfenate (CysSO) (section 1 of the Supporting Information). XANES simulations on the basis of Ni coordinations involving zero, one, or two Ni-bound oxygen atoms (section 2 of the Supporting Information) readily reproduced the shape changes between Ni-SR and Ni-B in the experimental spectra of the MBH due to the loss of the bridging hydroxyl species and suggested that the increased maximum in the XANES of Ni_{ia}-S reflects the presence of two non-μO oxygen ligands. By density functional theory calculations (DFT), geometry-optimized structures (not shown) were obtained for the Ni-B and Ni-S states with a standard $(CysS)_4$ ligation of Ni and with terminal or Ni−Fe bridging sulfenate groups (section 3 and Table S1 of the Supporting Information). The resulting structures suggest that terminal sulfenates bind to Ni via their S atom but equatorial bridging sulfenates bind to Ni via their O atom, in agreement with crystal data (section 1 of the Supporting Information). A bridging CysSO elongated the Ni−Fe distance to a value of ∼3 Å

Table 3. Ni EXAFS Simulation Parameters for PH and MBH[a]

		N_i (per Ni)/R_i (Å)/$2\sigma^2$ ($\times 10^3$ Å^2)			
sample	fit	Ni−O	Ni−S	Ni−Fe	R_F (%)
			PH		
Ni-A	I	0.82/1.85/4[b]	2.73[c]/2.16/5 1.27[c]/2.72/4[b]	1.00[b]/2.75/5[b]	11.2
Ni-C	II	0.13/1.83/4[b]	3.03[c]/2.18/7 0.97[c]/2.55/4[b]	1.00[b]/2.54/5[b]	15.3
Ni-SR	III	0.02/1.80/4[b]	3.23[c]/2.17/9 0.77[c]/2.56/4[b]	1.00[b]/2.51/5[b]	17.3
			MBH		
Ni-B	IV	0.67/1.88/4[b]	2.71[c]/2.20/14 1.29[c]/2.62/4[b]	1.00[b]/2.64/5[b]	12.1
Ni-SR	V	0.12/1.80/4[b]	3.07[c]/2.21/6 0.93[c]/2.60/4[b]	1.00[b]/2.58/5[b]	12.8
Ni_{ia}-S	VI	1.41/2.03/4[b]	2.30[c]/2.32/22 1.70[c]/2.98/4[b]	1.00[b]/3.05/5[b]	12.5

[a] State nominations follow attributions in Table 2. N_i is the coordination number, R_i the Ni−backscatterer distance, and $2\sigma_i^2$ the Debye−Waller factor. [b] Fixed parameters in the fit procedure. [c] The sum of the N_{Ni-S} values was restrained to 4. R_F was calculated for reduced distances of 1−2.5 Å. For approximate errors of R and N values, see the legend of Table 1.

and created an additional long Ni−sulfur distance. Similar changes were observed by XAS for the Ni_{ia}-S state of the MBH. Only minor changes in the Ni−Fe distance were observed for a terminal CysSO compared to a standard active site. These results favor a metal-bridging CysSO group in the Ni_{ia}-S state; however, a [NiFe] site structure without obvious cysteine modifications exists in the Ni-B state of the MBH.

DISCUSSION

Structure of FeS Clusters in the MBH. The Fe-XAS analysis suggests different FeS cluster compositions in MBH and PH. As a main result, a smaller number of Fe−Fe distances of ∼2.7 Å, typical for conventional [4Fe4S] and [3Fe4S] clusters,[21,90] was observed in the MBH. The small subunit of the PH contains two [4Fe4S] clusters in the proximal and distal positions relative to the active site and the medial [3Fe4S] cluster, respectively.[53] EPR spectroscopy revealed that the HoxK subunit of the MBH contains one [4Fe4S] cluster and one [3Fe4S] cluster, in addition to an unusual paramagnetic iron−sulfur species. The latter interacts magnetically with both the Ni(III) of the active site in the Ni-B state and the oxidized $[3Fe4S]^+$ cluster in the medial position.[43,45,54] Accordingly, this species most likely is located at the position of the proximal cluster. Similar EPR results were obtained for other O_2-tolerant [NiFe] H_2ases.[9,11,91,92] Site-directed mutagenesis studies of the MBH, combined with spectroscopic and electrochemical investigations, consistently point to a modified proximal FeS center, which has been shown to be crucially related to O_2 tolerance.[46,54] We therefore discuss possible structural motifs for this unusual cofactor, derived from the Fe-XAS analysis.

As emphasized previously, a common feature of the small subunits of O_2-tolerant membrane-bound [NiFe] H_2ases is the presence of two additional cysteine residues, Cys19 and Cys120

in the case of the MBH from *R. eutropha*, in the vicinity of the position of the proximal FeS cluster. These particular cysteine residues are replaced with glycines in standard H_2ases (see ref 54 and references cited therein). However, the four conserved cysteines, ligating the proximal cluster, are present both in standard [NiFe] H_2ases, such as the PH, and in the O_2-tolerant enzymes. Thus, the presence of two additional cysteine residues within coordination distance may provide a surplus of iron ligands in MBH-like O_2-tolerant H_2ases.

Fe-XAS revealed at most 6 Fe−Fe distances of 2.6−2.85 Å and up to 4 longer distances of ∼3.4 Å for the proximal cluster of the MBH. This is incompatible with a cubane [4Fe4S] species, for which 12 Fe−Fe distances of ∼2.7 Å would be expected and were actually found in the PH. We note that the error in the numbers of Fe−Fe distances in the MBH may be on the order of approximately ±2, due to statistical coupling between coordination number and Debye−Waller parameter in EXAFS simulations.[52] The aforementioned numbers of Fe−Fe interactions in the MBH suggest three Fe−Fe pairs with a separation of metal ions of 2.6−2.85 Å and one to two additional pairs with a separation of ∼3.4 Å. Fe−Fe distances longer than 4 Å cannot be excluded but are difficult to detect by XAS. Notably, there was no evidence from XAS of additional non-sulfur iron ligands in the MBH.

On the basis of these considerations, a similar ligation pattern of the conserved cysteines, assuming four proximal Fe ions in the MBH, and molecular modeling results of the structure of the HoxK subunit,[54] a possible model for the proximal FeS cluster is suggested (Figure 5A). It includes an Fe trimer combined with a more remote Fe ion. The shortest detected Fe−Fe distance of ∼2.6 Å suggests that one of the additional cysteines may provide a bridging ligand [Fe−μS(Cys)−Fe motif], as observed for the active site H-cluster of [FeFe] H_2ases.[27,30] However, it remains unclear if four μ_3S atoms are implemented in the structure and how the iron ∼3.4 Å from one or several of the other Fe ions is connected to the trimer. The loss of one μS bridge may open a coordination site at the more distant Fe ion for the binding of an additional cysteine. Notably, such a structure (Figure 5A) is conservative in a way that it comprises only iron ligated by sulfur ligands and requires relatively small deviations (<1 Å) of the Fe ions from the crystallographic positions in the PH.[53]

Modified FeS clusters were also observed in crystal structures of standard H_2ases, but mainly attributed to protein damage due to crystallization and/or X-ray-induced modifications during data collection.[93,94] The presence of a special cluster also in the most native, membrane-containing preparation,[43] the absence of X-ray-induced damage under our XAS conditions, and similar Fe-XAS data for various protein samples argue against unspecific FeS cluster modifications in the MBH. Furthermore, the MBH variant lacking the additional cysteines[54] reveals an iron coordination pattern more similar, although not fully identical, to that of the PH. Therefore, the data suggest a more cubane-like structure of the proximal cluster. This mutant enzyme exhibited a higher sensitivity to O_2 inhibition,[54] which correlates the presence of the two cysteines directly with the O_2 tolerance of the MBH.[46,54] Therefore, we propose that a structurally modified proximal FeS cluster is a native and functionally important feature of the MBH.

Properties of the [NiFe] Active Site. A central result of this Ni-XAS study is that the overall structural features of the functional states, Ni^{III}-B and Ni^{II}-SR, of the [NiFe] site in the MBH are similar to those in the PH (Figure 5B). Both revealed

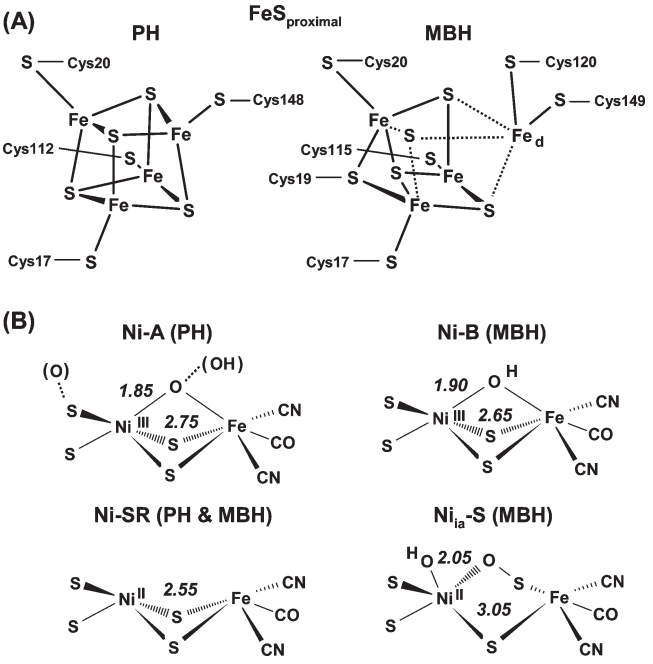

Figure 5. Structural motifs of FeS clusters and the [NiFe] site in PH and MBH. (A) Structure of the proximal [4Fe4S] cluster in crystallized PH[53] (left) and hypothetical structure of the proximal FeS cluster in MBH in agreement with the Fe-XAS results (right). The model was constructed from the PH structure by moving one iron (Fe_d) so that it was ∼3.4 Å from two other Fe ions. The particular positions of the two additional cysteines (C19 and C120) are plausible according to modeling results.[54] A bridging CysS may account for the shortest Fe−Fe distance of ∼2.6 Å. The connections of Fe_d to the other Fe ions by μS bonds and the presence of four such motifs are unclear (dotted lines). (B) Model structures of the [NiFe] site in agreement with the Ni-XAS results. The S atoms belong to cysteines; rounded Ni−Fe and first-sphere Ni−oxygen distances (in angstroms) are indicated. The iron is in the Fe(II) state. The Ni-B state is assigned to a bridging hydroxide.[54] The Ni-A state may be assigned either to a bridging OH^- group with a terminal CysSO or to a bridging hydroperoxide,[50,88,89] with the nonbridging O atoms relatively distant from Ni and not detectable by XAS. The location of the bridging CysSO in Ni_{ia}-S follows crystallographic data of standard H_2ases (section 1 of the Supporting Information), and the Ni-bound OH^- group is only tentative. Possible Ni-bound hydrogen species in Ni-SR were omitted.

four sulfur ligands at Ni, likely stemming from the four conserved cysteines at the active sites of both enzymes. For the Ni-B state of the MBH, a particularly short Ni−oxygen bond (Ni−μO motif) was detected, which we assign to a Ni−Fe bridging OH^- group as proposed for standard H_2ases.[50,76] A similar conclusion was reached in previous EPR and FTIR studies of the MBH.[43−45] Thus, major contributions to the O_2-tolerance of the MBH are not based on obvious modifications of its [NiFe] site.

There are, however, more subtle structural differences. The mean Ni−sulfur bond length was overall larger and a larger bond length distribution was observed, compared to that of the Ni-SR state of the MBH and those of the Ni-A and Ni-C states of the PH. The Ni coordination in the Ni-B state thus is considerably less homogeneous, possibly reflecting differences in the amino acid environment of the [NiFe] site. Indeed, at position 71 in the large subunit, a valine is found in the PH but a cysteine (C81) in the MBH.[44] The V71 side chain is ∼4 Å from the Ni−Fe bond bridging C68 in the PH.[50,53] C81 could be at a similar distance from

the bridging C78 in the MBH. In line with this rationale, mutations of C81 in the MBH negatively affected the affinity for the substrate H_2, but the O_2 tolerance remained unchanged.[26] A somewhat increased O_2 tolerance and a decreased affinity for carbon monoxide (CO), a common inhibitor of standard H_2ases but not of the MBH,[26] were found for a cysteine variant of the *Desulfovibrio fructosovorans* H_2ase.[13] Weak CO binding at Ni was also reported for the O_2-tolerant H_2ase of *Aquifex aeolicus*.[95] These results suggest that an additional cysteine close to the [NiFe] site is not sufficient to mediate full O_2 tolerance of the MBH. Rather, a fine-tuned [NiFe] site coordination may decrease the binding strength of inhibitory ligands of Ni. The longer Ni−μO bond and the shorter Ni−Fe distance suggest also that the bridging oxygen species in the Ni-B state of the MBH is less firmly bound than that in the Ni-A state of the PH. This interpretation would be even more interesting if the Ni-A state did not comprise a bridging peroxidic species, but rather a hydroxide (see below). Thus, a direct comparison of the Ni-B state of standard H_2ases with that of MBH by XAS would be appropriate. However, PH samples residing exclusively in the Ni-B state have not yet been purified, most probably because of overlapping redox potential windows for the Ni-B state and other states.[75,96,97]

In agreement with previous findings,[43,45,54] the inactive Ni-A state was not detected in any of the studied MBH samples, but Ni-A was the main species in the oxidized PH. Remarkably, the second oxygen atom of a bridging (hydro)peroxide (OOH^-) proposed for Ni-A could not be detected by Ni-XAS, meaning that it was either absent or farther from the Ni (Figure 5B) than the value of ~2.2 Å derived from crystal structures of standard H_2ases.[50,87] A second O atom could also be located on a terminal sulfenate group (section 1 of the Supporting Information).

MBH protein that was anaerobically oxidized prior to aerobic purification revealed the Ni-B state as the dominant site species. However, if this preparation was reduced with H_2 and subsequently reoxidized with air,[45,54] considerable amounts of the oxidatively modified Ni^{II}_{ia}-S species were found (Figure 5B). A similar observation was made for MBH samples that were purified completely aerobically.[43−45] According to the XAS and DFT results, this inactive state could feature a Ni−Fe bridging sulfenate group (Ni−O^-S_{Cys}−Fe motif), besides an additional Ni-bound oxygen species, possibly from OH^-. A similar CysSO bridge has been detected in crystals of standard H_2ases (section 1 of the Supporting Information). The occurrence of the Ni_{ia}-S state in purified MBH protein may be related to the redox status and/or integrity of its FeS clusters.[43−45,54] However, under physiological conditions, when the MBH is bound to the cytochrome *b* subunit in the membrane, the Ni_{ia}-S state has not been observed[43] and, hence, presumably is not functionally relevant.

Possible Clues about the O_2 Tolerance of the MBH of *R. eutropha*. The results of this study support the previously made conclusion[11,43,45,54] that a modified proximal FeS cluster, but not a modified [NiFe] site, is an essential prerequisite for O_2 tolerance in membrane-bound [NiFe] H_2ases. Likely, the key feature of the proximal cluster in the MBH is its altered redox potential compared to those of standard [NiFe] H_2ases,[43,46,54] which facilitates additional donation of electrons to the active site. Redox transitions of this cluster can be detected well by EPR.[43,45,98] Oxidation of at least one additional Fe ion in the MBH compared to the PH is indicated by our Fe-XANES results. In the absence of external electron donors and starting in a situation with fully reduced iron−sulfur centers, the proximal FeS cluster, the medial [3Fe4S] cluster, and the distal [4Fe4S] cluster of the MBH thus can provide at least three electrons to the [NiFe] active site, whereas only two electrons are provided by the distal [4Fe4S] and medial [3Fe4S] clusters of the PH. This difference may explain why the Ni-B state (Ni^{III}-OH^-), which formally is by one electron more reduced than Ni-A (Ni^{III}-O^-_{SCys}, OH^-, or Ni^{III}-OOH^-), is preferred in the MBH. A surplus electron acceptor capacity due to the oxidized proximal cluster, in addition to the oxidized distal [4Fe4S] and medial [3Fe4S] clusters, on the other hand also is in agreement with the observed Ni-SR formation after activation by hydrogen of the MBH in the Ni-B state.

These considerations support a mechanism for H_2 cleavage by the MBH in an oxygen-containing environment, including only Ni-B and the intermediates in the catalytic cycle (Ni-S, -C, and -SR).[33,54,98] During H_2 catalysis, the active MBH enzyme could provide electrons to reduce O_2 at the [NiFe] site to form the Ni-B state, which is rapidly reactivated. Thus, the catalytic activity is expected to depend on the relative concentrations of H_2 and O_2 and on the redox conditions controlling the availability of electrons.[11] The absence of the Ni-A state is common to all three O_2-tolerant [NiFe] H_2ases of *R. eutropha*.[24,43,85] Rapid O_2-induced Ni-A formation and slow reactivation of this state in O_2-sensitive H_2ases are major obstacles for their use in biotechnology. Thus, avoiding Ni-A formation is crucial for O_2-tolerant H_2 catalysis. Apparently, in the O_2-tolerant MBH, this goal mainly has been achieved by an enlarged reduction capacity for the active site due to a modified FeS cluster relay.

■ ASSOCIATED CONTENT

Supporting Information. Sulfenates in [NiFe] H_2ase crystal structures (section 1), XANES simulations (section 2), DFT calculations on [NiFe] active site models (section 3), and references. This material is available free of charge via the Internet at http://pubs.acs.org.

■ AUTHOR INFORMATION

Corresponding Author

*Freie Universität Berlin, FB Physik, Arnimallee 14, 14195 Berlin, Germany. Phone: +49 30 838 56101. Fax: +49 30 838 56299. E-mail: michael.haumann@fu-berlin.de.

Funding Sources

Financial support by the Deutsche Forschungsgemeinschaft (DFG) (SFB498-C1, -C8, and -C9; Ha3265/3-1 to M.H.; Unicat Cluster of Excellence Berlin), the EU/Energy Network SolarH2, and the Bundesministerium für Bildung and Forschung (Design Cells Consortium) is gratefully acknowledged. M.H. thanks the DFG for a Heisenberg Fellowship. A.L.D.L. thanks the Spanish MICIIN for financial support (Project CTQ2009-12649). M.S. is grateful to the Max Planck Society for the Advancement of Science for financial support.

■ ACKNOWLEDGMENT

We thank Drs. W. Meyer-Klaucke (EMBL at DESY) and F. Schäfers and M. Mertin (beamline KMC-1 at BESSY) for excellent technical support. M.H. thanks Prof. C. Limberg (Humboldt-Universität zu Berlin) for discussion and Dr. P. Chernev (Freie Universität Berlin) for providing GloFit. We thank T. Goris for his contributions to construction of the MBH mutant.

■ ABBREVIATIONS

EPR, electron paramagnetic resonance; EXAFS, extended X-ray absorption fine structure; DFT, density functional theory; PH, periplasmic [NiFe] H_2ase of *D. gigas*; FTIR, Fourier transform infrared spectroscopy; H_2ase, hydrogenase; MBH, membrane-bound [NiFe] H_2ase of *R. eutropha*; TXRF, total-reflection X-ray fluorescence analysis; XANES, X-ray absorption near-edge structure; XAS, X-ray absorption spectroscopy.

■ REFERENCES

(1) Special Issue on Hydrogenases (2007) *Chemical Reviews*, Vol. 107, American Chemical Society, Washington, DC.

(2) Cammack, R. F. M., and Robson, R., Eds. (1997) *Hydrogen as a fuel: Learning from Nature*, Taylor & Francis, London.

(3) Rittmann, B. E. (2008) Opportunities for renewable bioenergy using microorganisms. *Biotechnol. Bioeng. 100*, 203–212.

(4) Mertens, R., and Liese, A. (2004) Biotechnological applications of hydrogenases. *Curr. Opin. Biotechnol. 15*, 343–348.

(5) Antoni, D., Zverlov, V. V., and Schwarz, W. H. (2007) Biofuels from microbes. *Appl. Microbiol. Biotechnol. 77*, 23–35.

(6) Vincent, K. A., Parkin, A., Lenz, O., Albracht, S. P., Fontecilla-Camps, J. C., Cammack, R., Friedrich, B., and Armstrong, F. A. (2005) Electrochemical definitions of O_2 sensitivity and oxidative inactivation in hydrogenases. *J. Am. Chem. Soc. 127*, 18179–18189.

(7) Burgdorf, T., Lenz, O., Buhrke, T., van der Linden, E., Jones, A. K., Albracht, S. P., and Friedrich, B. (2005) [NiFe]-hydrogenases of *Ralstonia eutropha* H16: Modular enzymes for oxygen-tolerant biological hydrogen oxidation. *J. Mol. Microbiol. Biotechnol. 10*, 181–196.

(8) Guiral, M., Aubert, C., and Giudici-Orticoni, M. T. (2005) Hydrogen metabolism in the hyperthermophilic bacterium *Aquifex aeolicus*. *Biochem. Soc. Trans. 33*, 22–24.

(9) Yoon, K. S., Sakai, Y., Tsukada, N., Fujisawa, K., and Nishihara, H. (2009) Purification and biochemical characterization of a membrane-bound [NiFe]-hydrogenase from a hydrogen-oxidizing, lithotrophic bacterium, *Hydrogenophaga* sp. AH-24. *FEMS Microbiol. Lett. 290*, 114–120.

(10) Parkin, A., Goldet, G., Cavazza, C., Fontecilla-Camps, J. C., and Armstrong, F. A. (2008) The difference a Se makes? Oxygen-tolerant hydrogen production by the [NiFeSe]-hydrogenase from *Desulfomicrobium baculatum*. *J. Am. Chem. Soc. 130*, 13410–13416.

(11) Lukey, M. J., Parkin, A., Roessler, M. M., Murphy, B. J., Harmer, J., Palmer, T., Sargent, F., and Armstrong, F. A. (2010) How *Escherichia coli* is equipped to oxidize hydrogen under different redox conditions. *J. Biol. Chem. 285*, 3928–3938.

(12) Buhrke, T., Lenz, O., Krauss, N., and Friedrich, B. (2005) Oxygen tolerance of the H_2-sensing [NiFe] hydrogenase from *Ralstonia eutropha* H16 is based on limited access of oxygen to the active site. *J. Biol. Chem. 280*, 23791–23796.

(13) Liebgott, P. P., de Lacey, A. L., Burlat, B., Cournac, L., Richaud, P., Brugna, M., Fernandez, V. M., Guigliarelli, B., Rousset, M., Leger, C., and Dementin, S. (2011) Original design of an oxygen-tolerant [NiFe] hydrogenase: Major effect of a valine-to-cysteine mutation near the active site. *J. Am. Chem. Soc. 133*, 986–997.

(14) Dementin, S., Leroux, F., Cournac, L., de Lacey, A. L., Volbeda, A., Leger, C., Burlat, B., Martinez, N., Champ, S., Martin, L., Sanganas, O., Haumann, M., Fernandez, V. M., Guigliarelli, B., Fontecilla-Camps, J. C., and Rousset, M. (2009) Introduction of methionines in the gas channel makes [NiFe] hydrogenase aero-tolerant. *J. Am. Chem. Soc. 131*, 10156–10164.

(15) McTavish, H., Sayavedra-Soto, L. A., and Arp, D. J. (1995) Substitution of *Azotobacter vinelandii* hydrogenase small-subunit cysteines by serines can create insensitivity to inhibition by O_2 and preferentially damages H_2 oxidation over H_2 evolution. *J. Bacteriol. 177*, 3960–3964.

(16) Canaguier, S., Artero, V., and Fontecave, M. (2008) Modelling NiFe hydrogenases: Nickel-based electrocatalysts for hydrogen production. *Dalton Trans.*, 315–325.

(17) Rauchfuss, T. B. (2007) Chemistry. A promising mimic of hydrogenase activity. *Science 316*, 553–554.

(18) Lu, Y. (2006) Biosynthetic inorganic chemistry. *Angew. Chem., Int. Ed. 45*, 5588–5601.

(19) Bernhard, M., Buhrke, T., Bleijlevens, B., De Lacey, A. L., Fernandez, V. M., Albracht, S. P., and Friedrich, B. (2001) The H_2 sensor of *Ralstonia eutropha*. Biochemical characteristics, spectroscopic properties, and its interaction with a histidine protein kinase. *J. Biol. Chem. 276*, 15592–15597.

(20) Lenz, O., Bernhard, M., Buhrke, T., Schwartz, E., and Friedrich, B. (2002) The hydrogen-sensing apparatus in *Ralstonia eutropha*. *J. Mol. Microbiol. Biotechnol. 4*, 255–262.

(21) Buhrke, T., Löscher, S., Lenz, O., Schlodder, E., Zebger, I., Andersen, L. K., Hildebrandt, P., Meyer-Klaucke, W., Dau, H., Friedrich, B., and Haumann, M. (2005) Reduction of unusual iron-sulfur clusters in the H_2-sensing regulatory Ni-Fe hydrogenase from *Ralstonia eutropha* H16. *J. Biol. Chem. 280*, 19488–19495.

(22) van der Linden, E., Burgdorf, T., de Lacey, A. L., Buhrke, T., Scholte, M., Fernandez, V. M., Friedrich, B., and Albracht, S. P. (2006) An improved purification procedure for the soluble [NiFe]-hydrogenase of *Ralstonia eutropha*: New insights into its (in)stability and spectroscopic properties. *J. Biol. Inorg. Chem. 11*, 247–260.

(23) Burgdorf, T., Löscher, S., Liebisch, P., Van der Linden, E., Galander, M., Lendzian, F., Meyer-Klaucke, W., Albracht, S. P., Friedrich, B., Dau, H., and Haumann, M. (2005) Structural and oxidation-state changes at its nonstandard Ni-Fe site during activation of the NAD-reducing hydrogenase from *Ralstonia eutropha* detected by X-ray absorption, EPR, and FTIR spectroscopy. *J. Am. Chem. Soc. 127*, 576–592.

(24) Horch, M., Lauterbach, L., Saggu, M., Hildebrandt, P., Lendzian, F., Bittl, R., Lenz, O., and Zebger, I. (2010) Probing the active site of an O_2-tolerant NAD^+-reducing [NiFe]-hydrogenase from *Ralstonia eutropha* H16 by in situ EPR and FTIR spectroscopy. *Angew. Chem., Int. Ed. 49*, 8026–8029.

(25) Lenz, O., Gleiche, A., Strack, A., and Friedrich, B. (2005) Requirements for heterologous production of a complex metalloenzyme: The membrane-bound [NiFe] hydrogenase. *J. Bacteriol. 187*, 6590–6595.

(26) Ludwig, M., Cracknell, J. A., Vincent, K. A., Armstrong, F. A., and Lenz, O. (2009) Oxygen-tolerant H_2 oxidation by membrane-bound [NiFe] hydrogenases of *Ralstonia* species. Coping with low level H_2 in air. *J. Biol. Chem. 284*, 465–477.

(27) Fontecilla-Camps, J. C., Volbeda, A., Cavazza, C., and Nicolet, Y. (2007) Structure/function relationships of [NiFe]- and [FeFe]-hydrogenases. *Chem. Rev. 107*, 4273–4303.

(28) Armstrong, F. A., and Fontecilla-Camps, J. C. (2008) Biochemistry. A natural choice for activating hydrogen. *Science 321*, 498–499.

(29) Ermler, U., Grabarse, W., Shima, S., Goubeaud, M., and Thauer, R. K. (1998) Active sites of transition-metal enzymes with a focus on nickel. *Curr. Opin. Struct. Biol. 8*, 749–758.

(30) Peters, J. W. (1999) Structure and mechanism of iron-only hydrogenases. *Curr. Opin. Struct. Biol. 9*, 670–676.

(31) Bernhard, M., Benelli, B., Hochkoeppler, A., Zannoni, D., and Friedrich, B. (1997) Functional and structural role of the cytochrome *b* subunit of the membrane-bound hydrogenase complex of *Alcaligenes eutrophus* H16. *Eur. J. Biochem. 248*, 179–186.

(32) Friedrich, B., and Schwartz, E. (1993) Molecular biology of hydrogen utilization in aerobic chemolithotrophs. *Annu. Rev. Microbiol. 47*, 351–383.

(33) Cracknell, J. A., Wait, A. F., Lenz, O., Friedrich, B., and Armstrong, F. A. (2009) Kinetic and thermodynamic understanding of O_2 tolerance in [NiFe]-hydrogenases. *Proc. Natl. Acad. Sci. U. S. A. 106*, 20681–20686.

(34) Cracknell, J. A., Vincent, K. A., Ludwig, M., Lenz, O., Friedrich, B., and Armstrong, F. A. (2008) Enzymatic oxidation of H_2 in atmospheric O_2: The electrochemistry of energy generation from trace H_2 by aerobic microorganisms. *J. Am. Chem. Soc. 130*, 424–425.

(35) Vincent, K. A., Cracknell, J. A., Clark, J. R., Ludwig, M., Lenz, O., Friedrich, B., and Armstrong, F. A. (2006) Electricity from low-level

H_2 in still air: An ultimate test for an oxygen tolerant hydrogenase. *Chem. Commun.,* 5033–5035.

(36) Vincent, K. A., Cracknell, J. A., Lenz, O., Zebger, I., Friedrich, B., and Armstrong, F. A. (2005) Electrocatalytic hydrogen oxidation by an enzyme at high carbon monoxide or oxygen levels. *Proc. Natl. Acad. Sci. U.S.A. 102*, 16951–16954.

(37) Fernandez, V. M., Hatchikian, E. C., and Cammack, R. (1985) Properties and reactivation of 2 different deactivated forms of *Desulfovibrio gigas* hydrogenase. *Biochim. Biophys. Acta 832*, 69–79.

(38) Bleijlevens, B., van Broekhuizen, F. A., De Lacey, A. L., Roseboom, W., Fernandez, V. M., and Albracht, S. P. J. (2004) The activation of the [NiFe]-hydrogenase from *Allochromatium vinosum*. An infrared spectro-electrochemical study. *J. Biol. Inorg. Chem. 9*, 743–752.

(39) Kortlüke, C., Horstmann, K., Schwartz, E., Rohde, M., Binsack, R., and Friedrich, B. (1992) A gene complex coding for the membrane-bound hydrogenase of *Alcaligenes eutrophus* H16. *J. Bacteriol. 174*, 6277–6289.

(40) Ludwig, M. (2008) Ph.D. Thesis, Humboldt-Universität zu Berlin, Berlin.

(41) Volbeda, A., Charon, M. H., Piras, C., Hatchikian, E. C., Frey, M., and Fontecilla-Camps, J. C. (1995) Crystal structure of the nickel-iron hydrogenase from *Desulfovibrio gigas*. *Nature 373*, 580–587.

(42) De Lacey, A. L., Pardo, A., Fernandez, V. M., Dementin, S., Adryanczyk-Perrier, G., Hatchikian, E. C., and Rousset, M. (2004) FTIR spectroelectrochemical study of the activation and inactivation processes of [NiFe] hydrogenases: effects of solvent isotope replacement and site-directed mutagenesis. *J. Biol. Inorg. Chem. 9*, 636–642.

(43) Saggu, M., Zebger, I., Ludwig, M., Lenz, O., Friedrich, B., Hildebrandt, P., and Lendzian, F. (2009) Spectroscopic insights into the oxygen-tolerant membrane-associated [NiFe] hydrogenase of *Ralstonia eutropha* H16. *J. Biol. Chem. 284*, 16264–16276.

(44) Saggu, M., Ludwig, M., Friedrich, B., Hildebrandt, P., Bittl, R., Lendzian, F., Lenz, O., and Zebger, I. (2010) Impact of amino acid substitutions near the catalytic site on the spectral properties of an O_2-tolerant membrane-bound [NiFe] hydrogenase. *ChemPhysChem 11*, 1215–1224.

(45) Saggu, M., Teutloff, C., Ludwig, M., Brecht, M., Pandelia, M. E., Lenz, O., Friedrich, B., Lubitz, W., Hildebrandt, P., Lendzian, F., and Bittl, R. (2010) Comparison of the membrane-bound [NiFe] hydrogenases from *R. eutropha* H16 and *D. vulgaris* Miyazaki F in the oxidized ready state by pulsed EPR. *Phys. Chem. Chem. Phys. 12*, 2139–2148.

(46) Lenz, O., Ludwig, M., Schubert, T., Bürstel, I., Ganskow, S., Goris, T., Schwarze, A., and Friedrich, B. (2010) H_2 conversion in the presence of O_2 as performed by the membrane-bound [NiFe]-hydrogenase of *Ralstonia eutropha*. *ChemPhysChem 11*, 1107–1119.

(47) Bernhard, M., Schwartz, E., Rietdorf, J., and Friedrich, B. (1996) The *Alcaligenes eutrophus* membrane-bound hydrogenase gene locus encodes functions involved in maturation and electron transport coupling. *J. Bacteriol. 178*, 4522–4529.

(48) Schubert, T., Lenz, O., Krause, E., Volkmer, R., and Friedrich, B. (2007) Chaperones specific for the membrane-bound [NiFe]-hydrogenase interact with the Tat signal peptide of the small subunit precursor in *Ralstonia eutropha* H16. *Mol. Microbiol. 66*, 453–467.

(49) Ludwig, M., Schubert, T., Zebger, I., Wisitruangsakul, N., Saggu, M., Strack, A., Lenz, O., Hildebrandt, P., and Friedrich, B. (2009) Concerted action of two novel auxiliary proteins in assembly of the active site in a membrane-bound [NiFe] hydrogenase. *J. Biol. Chem. 284*, 2159–2168.

(50) Volbeda, A., Martin, L., Cavazza, C., Matho, M., Faber, B. W., Roseboom, W., Albracht, S. P. J., Garcin, E., Rousset, M., and Fontecilla-Camps, J. C. (2005) Structural differences between the ready and unready oxidized states of [NiFe] hydrogenases. *J. Biol. Inorg. Chem. 10*, 591–591.

(51) Strange, R. W., and Feiters, M. C. (2008) Biological X-ray absorption spectroscopy (BioXAS): A valuable tool for the study of trace elements in the life sciences. *Curr. Opin. Struct. Biol. 18*, 609–616.

(52) Dau, H., Liebisch, P., and Haumann, M. (2003) X-ray absorption spectroscopy to analyze nuclear geometry and electronic structure of biological metal centers: potential and questions examined with special focus on the tetra-nuclear manganese complex of oxygenic photosynthesis. *Anal. Bioanal. Chem. 376*, 562–583.

(53) Volbeda, A., Charon, M. H., Piras, C., Hatchikian, E. C., Frey, M., and Fontecilla-Camps, J. C. (1995) Crystal structure of the nickel-iron hydrogenase from *Desulfovibrio gigas*. *Nature 373*, 580–587.

(54) Goris, T. W., Wait, A. F., Saggu, M., Fritsch, J., Heidary, N., Stein, M., Zebger, I., Lendzian, F., Armstrong, F. A., Friedrich, B., and Lenz, O. (2011) A unique iron-sulfur cluster plays a crucial role in oxygen tolerance of a [NiFe] hydrogenase. *Nat. Struct. Biol. 7*, 310–318.

(55) Bradford, M. M. (1976) Rapid and sensitive method for quantitation of microgram quantities of protein utilizing principle of protein-dye binding. *Anal. Biochem. 72*, 248–254.

(56) Cammack, R., Fernandez, V. M., and Hatchikian, E. C. (1994) Nickel-iron hydrogenase. *Methods Enzymol. 243*, 43–68.

(57) Klockenkämper, R. (1996) *Total Reflection X-ray Fluorescence Analysis*, Wiley-VCH, London.

(58) Löscher, S., Burgdorf, T., Zebger, I., Hildebrandt, P., Dau, H., Friedrich, B., and Haumann, M. (2006) Bias from H_2 cleavage to production and coordination changes at the Ni-Fe active site in the NAD^+-reducing hydrogenase from *Ralstonia eutropha*. *Biochemistry 45*, 11658–11665.

(59) Stripp, S., Sanganas, O., Happe, T., and Haumann, M. (2009) The structure of the active site H-cluster of [FeFe] hydrogenase from the green alga *Chlamydomonas reinhardtii* studied by X-ray absorption spectroscopy. *Biochemistry 48*, 5042–5049.

(60) Gu, W., Jacquamet, L., Patil, D. S., Wang, H.-X., Evans, D. J., Smith, M. C., Millar, M., Koch, S., Eichhorn, D. M., Latimer, M., and Cramer, S. P. (2003) Refinement of the nickel site structure in *Desulfovibrio gigas* hydrogenase using range-extended EXAFS spectroscopy. *J. Inorg. Biochem. 93*, 41–51.

(61) Pettifer, R. F., and Hermes, C. (1985) Absolute energy calibration of X-ray-radiation from synchrotron sources. *J. Appl. Crystallogr. 18*, 404–412.

(62) Zabinsky, S. I., Rehr, J. J., Ankudinov, A. L., Albers, R. C., and Eller, M. J. (1995) Multiple-scattering calculations of X-ray-absorption spectra. *Phys. Rev. B 52*, 2995–3009.

(63) Löscher, S., Schwartz, L., Stein, M., Ott, S., and Haumann, M. (2007) Facilitated hydride binding in an Fe-Fe hydrogenase active-site biomimic revealed by X-ray absorption spectroscopy and DFT calculations. *Inorg. Chem. 46*, 11094–11105.

(64) Stein, M., and Lubitz, W. (2002) Quantum chemical calculations of [NiFe] hydrogenase. *Curr. Opin. Chem. Biol. 6*, 243–249.

(65) Siegbahn, P. E. M., Tye, J. W., and Hall, M. B. (2007) Computational studies of [NiFe] and [FeFe] hydrogenase. *Chem. Rev. 107*, 4414–4435.

(66) Neese, F. (2008) *ORCA: An ab initio density functional and semiempirical program package*, version 2.6-35, Universität Bonn, Bonn, Germany.

(67) Becke, A. D. (1988) Density-functional exchange-energy approximation with correct asymptotic behavior. *Phys. Rev. A 38*, 3098.

(68) Perdew, J. P. (1986) Density-functional approximation for the correlation energy of the inhomogeneous electron gas. *Phys. Rev. B 33*, 8822.

(69) Schäfer, A., Huber, C., and Ahlrichs, R. (1994) Fully optimized contracted Gaussian basis sets of triple ζ valence quality for atoms Li to Kr. *J. Chem. Phys. 100*, 5829–5835.

(70) Klamt, A., and Schüürmann, G. (1993) COSMO: A new approach to dielectric screening in solvents with explicit expressions for the screening energy and its gradient. *J. Chem. Soc. Perkin Trans. 2*, 799–805.

(71) Andzelm, J., Kölmel, C., and Klamt, A. (1995) Incorporation of solvation effects into density functional calculations of molecular energies and geometries. *J. Chem. Phys. 103*, 9312–9320.

(72) Westre, T. E., Kennepohl, P., DeWitt, J. G., Hedman, B., Hodgson, K. O., and Solomon, E. I. (1997) A multiplet analysis of Fe K-edge 1s $\rightarrow$ 3d pre-edge features of iron complexes. *J. Am. Chem. Soc. 119*, 6297–6314.

(73) Stiefel, E. I. G. G. N. (1994) Ferredoxins, hydrogenases, and nitrogenases: Metal-sulfide proteins. In *Bioinorganic Chemistry* (Bertine,

I. G. H. B., Lippard, S. J., and Valentine, J. S., Eds.) pp 365−453, University Science Books, Mill Valley, CA.

(74) Cammack, R., Fernandez, V. M., and Schneider, K. (1986) Activation and active-sites of nickel-containing hydrogenases. *Biochimie 68*, 85–91.

(75) Teixeira, M., Moura, I., Xavier, A. V., Moura, J. J. G., Legall, J., Dervartanian, D. V., Peck, H. D., and Huynh, B. H. (1989) Redox intermediates of *Desulfovibrio gigas* [NiFe] hydrogenase generated under hydrogen: Mössbauer and EPR characterization of the metal centers. *J. Biol. Chem. 264*, 16435–16450.

(76) Carepo, M., Tierney, D. L., Brondino, C. D., Yang, T. C., Pamplona, A., Telser, J., Moura, I., Moura, J. J. G., and Hoffman, B. M. (2002) O-17 ENDOR detection of a solvent-derived Ni-(OHx)-Fe bridge that is lost upon activation of the hydrogenase from *Desulfovibrio gigas*. *J. Am. Chem. Soc. 124*, 281–286.

(77) Brecht, M., van Gastel, M., Buhrke, T., Friedrich, B., and Lubitz, W. (2003) Direct detection of a hydrogen ligand in the [NiFe] center of the regulatory H_2-sensing hydrogenase from *Ralstonia eutropha* in its reduced state by HYSCORE and ENDOR spectroscopy. *J. Am. Chem. Soc. 125*, 13075–13083.

(78) Foerster, S., Stein, M., Brecht, M., Ogata, H., Higuchi, Y., and Lubitz, W. (2003) Single crystal EPR studies of the reduced active site of [NiFe] hydrogenase from *Desulfovibrio vulgaris* Miyazaki F. *J. Am. Chem. Soc. 125*, 83–93.

(79) Teixeira, M., Moura, I., Xavier, A. V., Dervartanian, D. V., Legall, J., Peck, H. D., Huynh, B. H., and Moura, J. J. G. (1983) *Desulfovibrio gigas* hydrogenase: redox properties of the nickel and iron-sulfur centers. *Eur. J. Biochem. 130*, 481–484.

(80) Niu, S., and Hall, N. B. (2001) Modeling the active sites in metalloenzymes 5. The heterolytic bond cleavage of H_2 in the [NiFe] hydrogenase of *Desulfovibrio gigas* by a nucleophilic addition mechanism. *Inorg. Chem. 40*, 6201–6203.

(81) Wisitruangsakul, N., Lenz, O., Ludwig, M., Friedrich, B., Lendzian, F., Hildebrandt, P., and Zebger, I. (2009) Monitoring catalysis of the membrane-bound hydrogenase from *Ralstonia eutropha* H16 by surface-enhanced IR absorption spectroscopy. *Angew. Chem., Int. Ed. 48*, 611–613.

(82) Colpas, G. J., Maroney, M. J., Bagyinka, C., Kumar, M., Willis, W. S., Suib, S. L., Mascharak, P. K., and Baidya, N. (1991) X-ray spectroscopic studies of nickel complexes, with application to the structure of nickel sites in hydrogenases. *Inorg. Chem. 30*, 920–928.

(83) Davidson, G., Choudhury, S. B., Gu, Z., Bose, K., Roseboom, W., Albracht, S. P., and Maroney, M. J. (2000) Structural examination of the nickel site in *Chromatium vinosum* hydrogenase: Redox state oscillations and structural changes accompanying reductive activation and CO binding. *Biochemistry 39*, 7468–7479.

(84) Gu, Z. J., Dong, J., Allan, C. B., Choudhury, S. B., Franco, R., Moura, J. J. G., LeGall, J., Przybyla, A. E., Roseboom, W., Albracht, S. P. J., Axley, M. J., Scott, R. A., and Maroney, M. J. (1996) Structure of the Ni sites in hydrogenases by X-ray absorption spectroscopy. Species variation and the effects of redox poise. *J. Am. Chem. Soc. 118*, 11155–11165.

(85) Löscher, S., Gebler, A., Stein, M., Sanganas, O., Buhrke, T., Zebger, I., Dau, H., Friedrich, B., Lenz, O., and Haumann, M. (2010) Protein-protein complex formation affects the Ni-Fe and Fe-S centers in the H_2-sensing regulatory hydrogenase from *Ralstonia eutropha* H16. *ChemPhysChem 11*, 1297–1306.

(86) Leroux, F., Dementin, S., Burlatt, B., Cournac, L., Volbeda, A., Champ, S., Martin, L., Guigliarelli, B., Bertrand, P., Fontecilla-Camps, J., Rousset, M., and Leger, C. (2008) Experimental approaches to kinetics of gas diffusion in hydrogenase. *Proc. Natl. Acad. Sci. U.S.A. 105*, 11188–11193.

(87) Ogata, H., Hirota, S., Nakahara, A., Komori, H., Shibata, N., Kato, T., Kano, K., and Higuchi, Y. (2005) Activation process of [NiFe] hydrogenase elucidated by high-resolution X-ray analyses: conversion of the ready to the unready state. *Structure 13*, 1635–1642.

(88) Higuchi, Y., Ogata, H., Miki, K., Yasuoka, N., and Yagi, T. (1999) Removal of the bridging ligand atom in the Ni-Fe active site of [NiFe] hydrogenase upon reduction with H_2, as revealed by X-ray structure analysis at 1.4 Å resolution. *Structure 7*, 549–557.

(89) Happe, R. P., Roseboom, W., Pierik, A. J., Albracht, S. P. J., and Bagley, K. A. (1997) Biological activation of hydrogen. *Nature 385*, 126–126.

(90) Beinert, H., Holm, R. H., and Munck, E. (1997) Iron-sulfur clusters: Nature's modular, multipurpose structures. *Science 277*, 653–659.

(91) Knüttel, K. S. K., Erkens, A., Plass, W., Müller, A., Bill, E., and Trautwein, A. X. (1994) Redox properties of the metal centers in membrane-bound hydrogenase from *Alcaligenes eutrophus*. *Bull. Pol. Acad. Sci., Chem. 42*, 495–511.

(92) Pandelia, M. E., Fourmond, V., Tron-Infossi, P., Lojou, E., Bertrand, P., Leger, C., Giudici-Orticoni, M. T., and Lubitz, W. (2010) Membrane-bound hydrogenase I from the hyperthermophilic bacterium *Aquifex aeolicus*: Enzyme activation, redox intermediates and oxygen tolerance. *J. Am. Chem. Soc. 132*, 6991–7004.

(93) Ogata, H., Kellers, P., and Lubitz, W. (2010) The crystal structure of the [NiFe] hydrogenase from the photosynthetic bacterium *Allochromatium vinosum*: Characterization of the oxidized enzyme (Ni-A state). *J. Mol. Biol. 402*, 428–444.

(94) Matias, P. M., Soares, C. M., Saraiva, L. M., Coelho, R., Morais, J., Le Gall, J., and Carrondo, M. A. (2001) [NiFe] hydrogenase from *Desulfovibrio desulfuricans* ATCC 27774: gene sequencing, three-dimensional structure determination and refinement at 1.8 Å and modelling studies of its interaction with the tetrahaem cytochrome c_3. *J. Biol. Inorg. Chem. 6*, 63–81.

(95) Pandelia, M. E., Infossi, P., Giudici-Orticoni, M. T., and Lubitz, W. (2010) The oxygen-tolerant hydrogenase I from *Aquifex aeolicus* weakly interacts with carbon monoxide: An electrochemical and time-resolved FTIR study. *Biochemistry 49*, 8873–8881.

(96) Roberts, L. M., and Lindahl, P. A. (1994) Analysis of oxidative titrations of *Desulfovibrio gigas* hydrogenase; implications for the catalytic mechanism. *Biochemistry 33*, 14339–14350.

(97) Dole, F., Fournel, A., Magro, V., Hatchikian, E. C., Bertrand, P., and Guigliarelli, B. (1997) Nature and electronic structure of the Ni-X dinuclear center of *Desulfovibrio gigas* hydrogenase. Implications for the enzymatic mechanism. *Biochemistry 36*, 7847–7854.

(98) Pandelia, M. E., Nitschke, W., Infossi, P., Giudici-Orticoni, M. T., Bill, E., and Lubitz, W. (2011) Characterization of a unique [FeS] cluster in the electron transfer chain of the oxygen tolerant [NiFe] hydrogenase from *Aquifex aeolicus*. *Proc. Natl. Acad. Sci. U.S.A. 108*, 6097–6102.